A New Time-Effective Weighted Interpolation Method for Color Filter Array Demosaicking

Yuxuan Song(✉)

Hanhong College, Southwest University, Chongqing, China
songyuxuanswu@163.com

Abstract. To reduce the cost of storage and size, most digital cameras capture images through a chip whose surface is covered with a color filter array (CFA) where each sensor only samples one of three original color values. To reconstruct a full image, an interpolation process, often called CFA demosaicking, is required to estimate the missing color values. In this paper, a new time-effective weighted interpolation method for CFA demosaicking is proposed. The new algorithm contains three consecutive steps: First, during the interpolation of green plane, the image is divided into three different regions where each of these is handled with different strategies. Second, four-directional weighted interpolation with gradient inverse weighted filtering (GIWF) refinement is utilized in filling the missing red and blue components. Finally, a postprocessing step with 2-dimensional finite impulse response (FIR) filter is used for further enhancement. An analysis of experimental results shows that the proposed algorithm inherits the good traits of edge preservation under lower time cost.

Keywords: Color Filter Array (CFA) Demosaicking · Weighted Interpolation · Finite Impulse Response (FIR) Filter

1 Introduction

On account of decrease in storage and size, most digital cameras have employed a single-chip CCD (charge coupled device) or CMOS (complementary metal oxide semiconductor) sensor for image acquisition, whose surface is covered by a color filter array (CFA). Generally, a CFA is consisted of a set of spectrally specific filters in staggered arrangement, where each sensor simply samples one of the three original color values. To rebuild the full image from these sparsely sampled pixel values, an interpolation process is required for the estimation of missing color components at each pixel, taking advantage of information of its nearby pixels. Such a process is called CFA interpolation or demosaicking [1, 4]. Figure 1 shows the Bayer pattern, the most typical CFA.

In pursuit of higher interpolation accuracy and better preservation of sensitive edge and texture details for human visual system (HVM), many different demosaicking methods have been proposed. Edge-directed interpolation methods [9, 11] considering the optical correlation of adjacent pixel values along the predefined directions, are outstanding in the preservation of the edge information and modest computing complexity. In

D. Qiu et al. (Eds.): ICBBEM 2022, AHIS 5, pp. 945–956, 2023.
https://doi.org/10.2991/978-94-6463-030-5_93

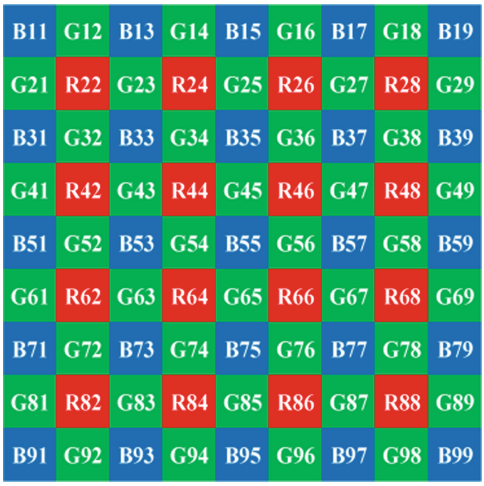

Fig. 1. 9 × 9 Bayer CFA.

parametric interpolation methods [5, 12], the unavailable color components are estimated by filters with coefficients determined by the self-similarity of neighboring color values, which is efficient for the restoration of images with large area of smooth regions. Some other methods like the applications of frequency domain [2, 8] and deep neural network [3, 13] also have impressive performance; however, due to the complexity of computation and circuit achievement, it is inappropriate to apply these methods to real-time situations. Thus, in this paper, an amelioration of the combination of edge-based and parametric demosaicking methods is proposed.

In a CFA image, the number of green pixels is approximately as twice many as that of blue and green pixels. Besides, HVS is most sensitive to green color. Therefore, to reduce the time complexity with the lowest decrease in the accuracy, it can be achievable to make modifications to the interpolation of green plane. In this paper, CFA sample is divided into smooth, regular and complex regions. High-quality interpolation [5] is applied to smooth regions and four-directional interpolation method is processed on regular regions. With the purpose of presenting texture details, eight-directional interpolation is employed in complex regions. Later, in the interpolation of blue and red components, four-directional weighted interpolation is adopted. Exceptionally, gradient inverse weighted filtering (GIWF) [10] is utilized to improve the accuracy of the interpolated. Finally, a postprocessing step with 2-dimensional antialiasing finite impulse response (FIR) filter induces the realignment of color planes, marking the end of the whole CFA demosaicking.

The rest of the paper is organized as follows. In Sect. 2, the process of time-effective weighted interpolation (TEWI) is depicted. Later, an analysis of performance of TEWI is illustrated in Sect. 3. Finally, a conclusion is drawn in Sect. 4.

2 Process of Proposed Algorithm

It is manifest to know that in a typical Bayer pattern CFA, pixels with green components outnumber those with blue or red components two to one and therefore contain the largest volume of information of the image. Additionally, HVS is testified to be most sensitive to green components. Consequently, the interpolation of green pixels is first carried out. After the interpolation of green plane, blue and red components are restored based on the original information of CFA image and the interpolated in former steps. Finally, a postprocessing step with 2-dimensional FIR filter is used.

2.1 Interpolation of Missing Green Components

To reduce the running time with the smallest discount of the accuracy, CFA sample is divided into three regions with the help of nearby color difference (NCD) defined as

$$\begin{aligned} NCD(i,j) = &|\beta(i-1,j) - \beta(i+1,j)| \\ &+ |\beta(i-1,j+1) - \beta(i+1,j-1)| \\ &+ |\beta(i-1,j-1) - \beta(i+1,j+1)| + |\beta(i,j-1) - \beta(i,j+1)|, \end{aligned} \tag{1}$$

where β represents the Bayer image, i, j represents the line and column indices. Two NCDs are needed for the division. Theoretically, the parameters should be gained by training according to the content of images. For convenience, the NCDs are experimentally given as 20 and 80 here.

For regions with NCDs lower than 20, they are called smooth regions. Empirically and experimentally, over seventy percent of an image are regarded as being smooth. Therefore, due to low computational complexity, high-quality interpolation [5] as shown in Fig. 2(a) is hired by smooth regions for green plane recovery. Regions whose NCDs varying from 20 to 80 are interpreted as regular regions, where the interpolation of green plane is achieved by four-directional weighted interpolation method [9] as symbolized in Fig. 2(b).

The most fragile areas during image reconstruction are located in complex regions whose NCDs are above 80. A detailed description of eight-directional interpolation procedure applied here is exemplified by the calculation of G at B_{55} position as shown in Fig. 2(c).

The missing G component $\tilde{G}_{B55}$ at B_{55} is first estimated along eight directions: N, S, W, E, NW, NE, SW, and SE, where the estimated values can be obtained according to [4], denoted by $\tilde{G}^{N}_{B55}$, $\tilde{G}^{S}_{B55}$, $\tilde{G}^{W}_{B55}$, $\tilde{G}^{E}_{B55}$, $\tilde{G}^{NW}_{B55}$, $\tilde{G}^{NE}_{B55}$, $\tilde{G}^{SW}_{B55}$, $\tilde{G}^{SE}_{B55}$. Then, more reliable directional gradient factors along eight directions are calculated as

$$\begin{aligned} \nabla^{N} = &|G_{54} - G_{34}| + |R_{44} - R_{24}| + |B_{55} - B_{35}| + |G_{45} - G_{25}| \\ &+ |R_{46} - R_{26}| + ||B_{55} - G_{45}| - |G_{45} - B_{35}||, \end{aligned} \tag{2}$$

$$\begin{aligned} \nabla^{S} = &|G_{54} - G_{74}| + |R_{64} - R_{84}| + |B_{55} - B_{75}| + |G_{65} - G_{85}| + |G_{56} - G_{76}| \\ &+ |R_{66} - R_{86}| + ||B_{55} - G_{65}| - |G_{65} - B_{75}||, \end{aligned} \tag{3}$$

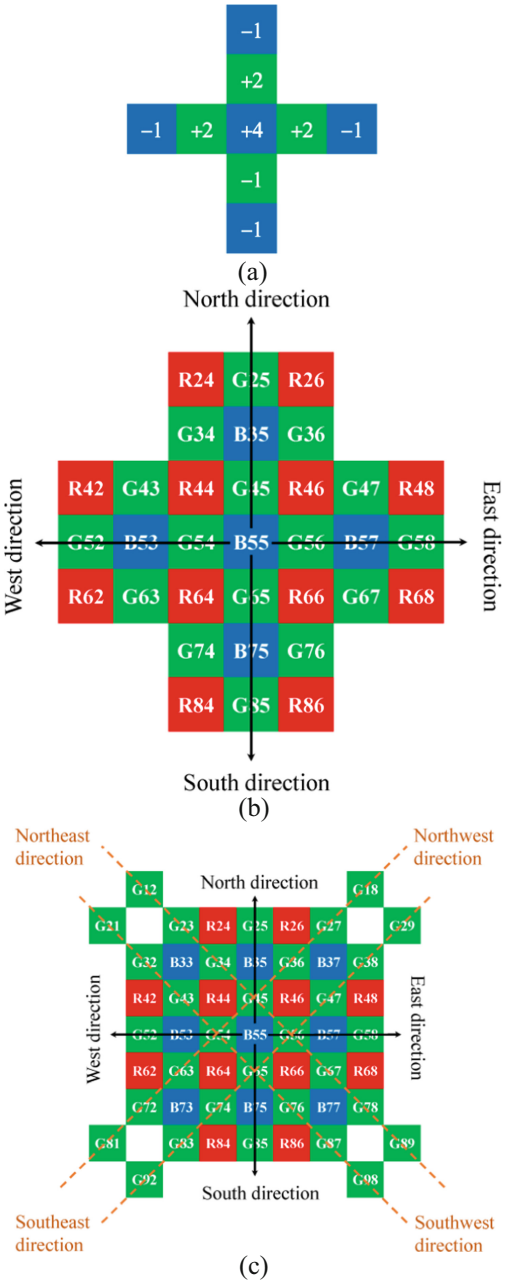

Fig. 2. (a) High-quality interpolation, (b) four-directional interpolation and (c) eight-directional interpolation of G at B locations. The interpolation of G at R locations is the same after replacing the B pixels with R pixels.

$$\nabla^W = |G_{45} - G_{43}| + |R_{44} - R_{42}| + |B_{55} - B_{53}| + |G_{54} - G_{52}| + |G_{65} - G_{63}| + |R_{64} - R_{62}| + ||B_{55} - G_{54}| - |G_{54} - B_{53}||, \tag{4}$$

$$\nabla^E = |G_{45} - G_{47}| + |R_{46} - R_{48}| + |B_{55} - B_{57}| + |G_{56} - G_{58}| + |G_{65} - G_{67}| + |R_{66} - R_{68}| + ||B_{55} - G_{56}| - |G_{56} - B_{57}||, \tag{5}$$

$$\nabla^{NW} = |G_{56} - G_{45}| + |G_{45} - G_{34}| + |G_{34} - G_{23}| + |G_{65} - G_{54}| + |G_{54} - G_{43}| + |G_{43} - G_{32}| + |B_{55} - B_{33}|, \tag{6}$$

$$\nabla^{NE} = |G_{54} - G_{45}| + |G_{45} - G_{36}| + |G_{36} - G_{27}| + |G_{65} - G_{56}| + |G_{56} - G_{47}| + |G_{47} - G_{38}| + |B_{55} - B_{37}|, \tag{7}$$

$$\nabla^{SW} = |G_{45} - G_{54}| + |G_{54} - G_{63}| + |G_{63} - G_{72}| + |G_{56} - G_{65}| + |G_{65} - G_{74}| + |G_{74} - G_{83}| + |B_{55} - B_{73}|, \tag{8}$$

$$\nabla^{SE} = |G_{45} - G_{56}| + |G_{56} - G_{67}| + |G_{67} - G_{78}| + |G_{54} - G_{65}| + |G_{65} - G_{76}| + |G_{76} - G_{87}| + |B_{55} - B_{77}|. \tag{9}$$

To avoid potential error, the estimated values along the eight directions are combined as follows, with the weighted sum denoted by $\tilde{G}^i_{B55}$

$$\tilde{G}^i_{B55} = \sum_{k=\{N,S,W,E,NW,NE,SW,SE\}} \tilde{G}^k_{B55} \frac{1}{\nabla^k + \varepsilon}, \tag{10}$$

where ε is a small positive number to avoid the denominator's being zero.

Because of the high correlation between $\tilde{G}_{B55}$ and its four nearby pixels G_{45}, G_{65}, G_{54} and G_{56} along level and vertical directions as shown in Fig. 3(a), the GIWF [11] method is utilized to refine $\tilde{G}^i_{B55}$ to obtain $\tilde{G}_{B55}$ as follows.

$$\tilde{G}_{B55} = 0.5 \times \tilde{G}^i_{B55} + 0.5 \times \frac{\sum \Delta_k \times w_k}{\sum w_k}, \tag{11}$$

$$\Delta_k = G_k - \tilde{G}^i_{B55}, \quad w_k = \frac{1}{1 + |\Delta_k|}, \tag{12}$$

where $k = \{45, 65, 54, 56\}$ and k represents four nearby existing G pixel values around B_{55}.

2.2 Interpolation of Missing Blue and Red Components

In Sect. 2.1, green pixels are interpolated by using the proposed approach. Considering the high correlation across R, G and B planes, the interpolation process for the missing R and B components is first accomplished by DWI method used in [3] as shown in Fig. 4(a) and Fig. 4(b), obtaining B^i s and R^i s. Similar to the refinement process in Sect. 2.1, GIWF method is applied again, calculating out the final $\tilde{B}$ s and $\tilde{R}$ s.

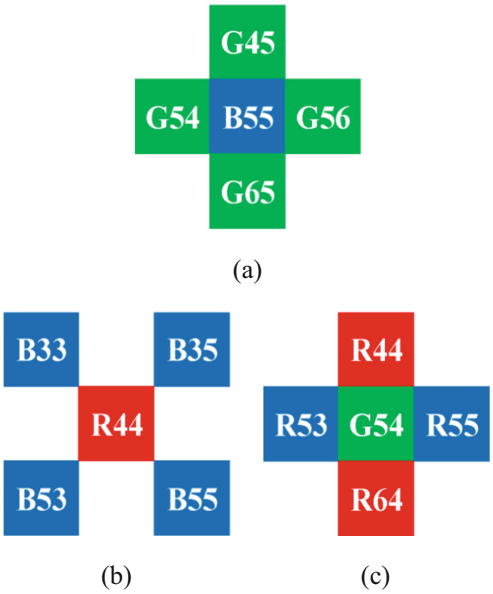

Fig. 3. Gradient inverse weighted filtering (GIWF) of (a) G at B locations, (b) B at R locations and (c) R at G locations.

2.3 Postprocessing

The bothering artifacts are induced by the inclusion of untrustworthy and less rigid correlation during the interpolation of red and blue planes [11]. Therefore, an additional postprocessing step is expected to fix the correlation over three color planes. In the framework of proposed postprocessing, the updating of green samples comes at first with the use of color differences between red and green (D_{GR}) and blue and green (D_{GB}). Given a 5 × 5 sliding window (D_{GR} [i – 2: i + 2, j – 2: j + 2]) surrounding the central pixel (D_{GR} [i, j]) as shown in right half of Fig. 5, values of color differences in the sliding window are multiplied by a 2-dimensional antialiasing FIR filter as shown in left half of Fig. 5, obtaining the updated color difference $\tilde{D}_{GR}$. This scheme is also available to refine color differences $\tilde{D}_{GB}$, $\tilde{D}_{RG}$ and $\tilde{D}_{BG}$. Specifically, the final updated green pixel value is obtained with $\tilde{D}_{GB}$ and demosaicked $\tilde{R}$ and $\tilde{B}$ in Sect. 2.2.

$$\tilde{G} = 0.5 \times \left(\tilde{D}_{GR} + \tilde{R}\right) + 0.5 \times \left(\tilde{D}_{GB} + \tilde{B}\right). \tag{13}$$

After the modification of green plane, the refinement of red and blue color planes with $\tilde{D}_{RG}$ and $\tilde{D}_{BG}$ is

$$\tilde{R} = \tilde{G} + \tilde{D}_{RG}, \quad \tilde{B} = \tilde{G} + \tilde{D}_{BG} \tag{14}$$

With all color planes $[\tilde{R}, \tilde{G}, \tilde{B}]$ successfully gained, the full image is finally demosaicked.

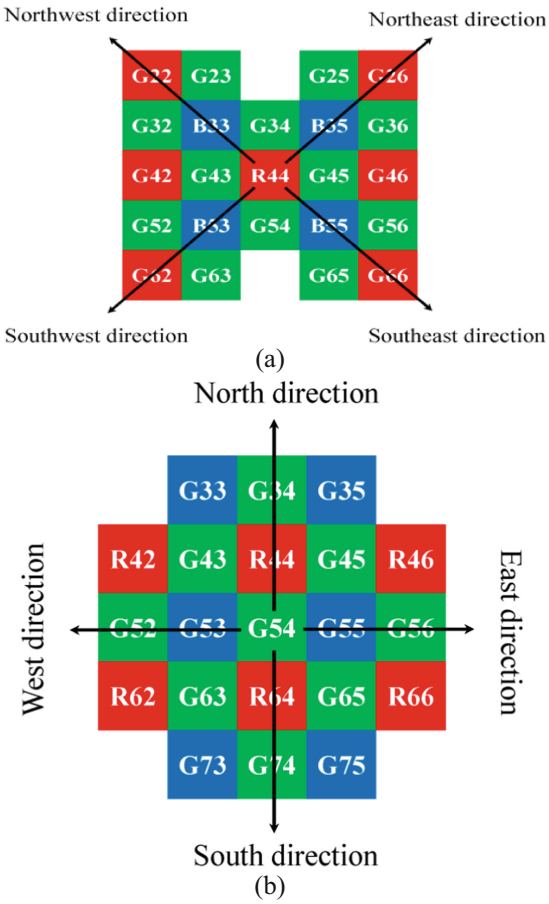

Fig. 4. Four-directional interpolation of (a) B at R locations and (b) R at G locations. The letters starting with a "G" in the blocks whose colors are not green indicate the interpolated G at R or B positions during the interpolation of missing G components, which are utilized in the interpolation of missing R or B components.

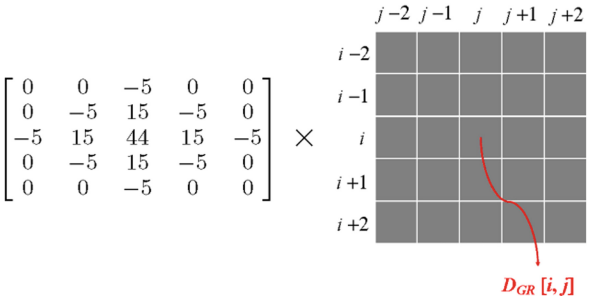

Fig. 5. Postprocessing. The red string in the right half of the figure indicates the central pixel in the 5 × 5 sliding window symbolized by grey shades.

Fig. 6. Cropped McM subimages used in the experiments, which are labeled #1–#18 from top to bottom and left to right. (photo credit: Original)

3 Experimental Results

McMaster (McM) color images have lower spectral correlations and are close to the sampled images captured by optical sensors. Figure 6 shows 18 subimages in the McM data set [7]. Experiments of CFA demosaicking with BI, Luo et al. [12], HI [5], DWI (Lu et al. 2003), MDWI [11] and TEWI are conducted using MATLAB 2020a with a processor of Inter (R) Core (TM) i5-10210U CPU @ 1.60 GHZ.

3.1 Objective Evaluation

Color peak signal-to-noise ratio (CPSNR) [6], eligible for describing the intensity difference between original images and demosaicked images, is exploited for the objective evaluation of the demosaicked images and is introduced as

$$CMSE = \frac{\sum\limits_{k=\{R,G,B\}} \sum\limits_{i=1}^{W} \sum\limits_{j=1}^{H} (I_{i,j,k} - \tilde{I}_{i,j,k})^2}{3 \times W \times H}, \tag{15}$$

$$CPSNR = 10 \times \lg\left(\frac{255^2}{CMSE}\right), \tag{16}$$

where CMSE denotes the color mean square error between the original image I and the demosaicked image in R, G and B channels within the size of the image $W \times H$. It is evident that when the CMSE approaches zero, the CPSNR is closer to the positive infinity. Thus, demosaicking method with higher CPSNR produces images in higher quality and vice versa.

Table 1 presents the comparison of the objective image quality measured by the CPSNR in decibels of six methods and running time in seconds of MDWI and TEWI. To compare intuitively, the average CPSNR and time are given. For the CPSNR, TEWI method has good performance in most of the images in the McM data set. Specifically, for images #1, #5, #6, #9, #15, #16, #17, TEWI yields much higher CPSNR than other methods. Despite of small decreases of the CPSNR in the other 11 images and the average level compared with MDWI, the good trait of high interpolation accuracy is preserved by TEWI. For the running time, statistics in both the single images and the average level undeniably demonstrate its excellent time efficiency, where the processing time of MDWI is reduced by over 80% in TEWI.

Table 1. Comparison of the CPSNR (In Decibels) and Processing Time (In Seconds) with Different Demosaicking Methods

Image	CPSNR						Processing Time	
	HI	*Luo et al.*	*HI*	*DWI*	*MDWI*	*TEWI*	*MDWI*	*TEWI*
1	27.0144	26.5030	27.0831	28.0643	29.1149	29.2094	0.9516	0.1991
2	30.9698	32.0915	33.0155	34.0886	34.7985	34.6103	0.9501	0.1837
3	26.3453	29.7653	31.0720	32.6942	32.2932	31.5739	0.9444	0.2012
4	28.0595	32.0754	33.7577	36.8952	36.8035	35.9431	0.9428	0.1823
5	31.8942	31.3044	31.9734	32.7239	34.2271	34.3983	0.8809	0.1775
6	36.0206	34.4065	35.2248	35.8474	37.9853	38.2410	0.9764	0.1961
7	30.1897	33.8519	35.0076	35.9102	35.1124	34.3084	0.9983	0.1724
8	31.1292	34.1279	35.8087	36.6824	36.8901	36.2829	0.9772	0.1664
9	32.8489	33.8781	34.8375	35.5020	36.9506	36.9652	0.9853	0.1812
10	35.1794	35.6224	36.6305	37.2628	38.4229	38.3991	0.9530	0.1657
11	36.5321	36.5294	37.4652	38.1300	39.5711	39.5462	0.9356	0.1783
12	32.7373	34.5030	36.0928	37.3790	38.2015	37.8967	0.9701	0.1662
13	37.1899	37.8270	38.7760	39.9687	40.9585	40.8918	0.9752	0.1895
14	35.9195	36.3559	36.9601	37.8332	38.7960	38.6917	0.9764	0.1633
15	36.7363	36.7506	37.4135	37.9254	39.1671	39.2584	0.9672	0.1658
16	31.0499	29.7792	30.9813	31.9515	34.2868	34.8163	0.9337	0.1937
17	32.5248	30.4358	31.0404	31.5619	33.0657	33.5282	0.9400	0.1956
18	29.4994	31.2140	32.7168	34.6246	35.6574	35.5197	1.1650	0.1987
Avg.	**32.3245**	**33.1679**	**34.2143**	**35.2801**	**36.2390**	**36.1156**	**0.9680**	**0.1820**

3.2 Subjective Evaluation

To subjectively evaluate the performance, partially zoomed images of the two specific images labeled #13 and #17 are used to depict the excellence in preserving detail information of TEWI. In Fig. 7(a), a partially zoomed image of the sun from image #13 shows the ability of preserving regular details. Compared Fig. 7(g) with Fig. 7(e), the image recovered by TEWI eliminates a large share of salt noise-like white artifacts in the image processed with DWI. With Fig. 7(f) joining the comparison, TEWI is certain for better eligibility of color compensation, proven by the fact that TEWI undermines the contrast ratios within the boundaries of sunbeams in the image demosaicked by MDWI. Besides, to further evaluate the irregular detail recovery performance of TEWI, a partially zoomed image of flowers from image #17 as shown in Fig. 8(a) is selected. After demosaicking, the image rebuilt by TEWI produces the least artifacts among the compared algorithms. Not only does TEWI reduce the number of black artifacts on the edges of red petals but also it enlarges green regions of leaves in the images demosaicked by DWI and MDWI.

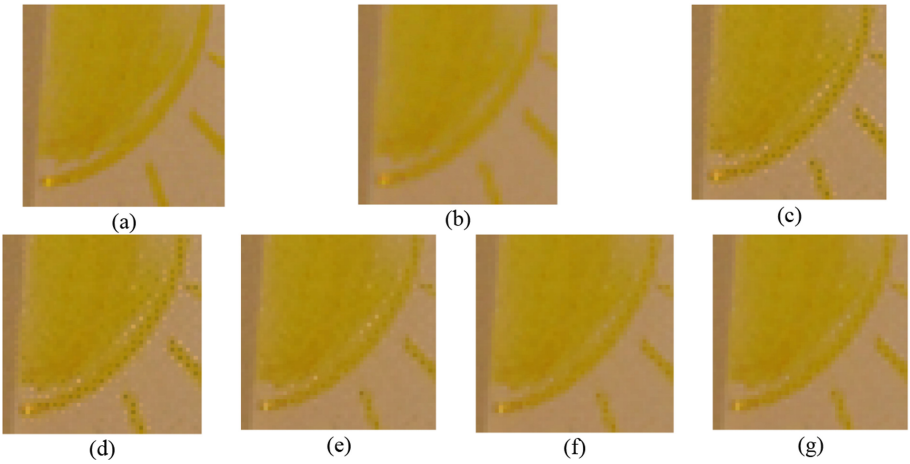

Fig. 7. (a) Original image #13 from the McM image data set and the reconstructed images by different demosaicking algorithms: (b) BI, (c) Luo et al., (d) HI, (e) DWI, (f) MDWI, (g) TEWI.

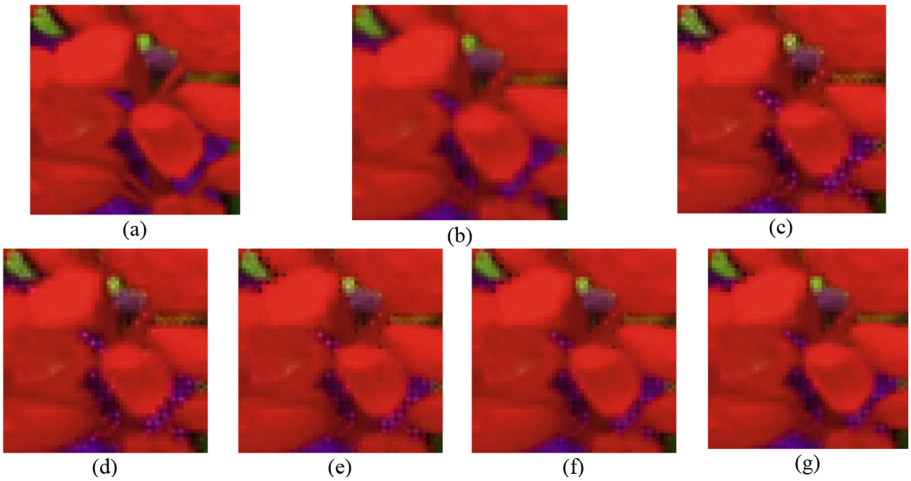

Fig. 8. (a) Original image #17 from the McM image data set and the reconstructed images by different demosaicking algorithms: (b) BI, (c) Luo et al., (d) HI, (e) DWI, (f) MDWI, (g) TEWI.

Through objective and subjective evaluations, that TEWI owns the overwhelming time efficiency and inherits outstanding traits of preserving edges and details from MDWI is verified. Undoubtedly, TEWI gives birth to favorable full-color images with well-eliminated artifacts under reduced temporal complexity.

4 Conclusion

In this paper, a new time-effective weighted interpolation method that combines parametric, edge-directed interpolation method, GIWF method and postprocessing with 2-dimensional FIR filter is proposed. There are three steps of the proposed TEWI method. First, with the help of NCD, the image is divided into smooth, regular and complex regions. For the interpolation of green plane in smooth regions, high-quality interpolation method is adopted. Four-directional weighted interpolation method is required for the restoration of green components in regular regions. Complex regions that appear to be the most fragile, are processed by an eight-directional weighted interpolation. Second, the interpolation of red and blue planes is achieved by four-directional weighted interpolation. In the first two steps, GIWF method is utilized for enhancing the spatial correlation. Finally, a postprocessing step with 2-directional FIR filter is qualified for fixing the irrational correlations. Experiments with five existing methods and TEWI are conducted on the McM data set, whose results objectively and subjectively authenticate that TEWI attempts to rebuild favorable full-color images with higher time efficiency.

References

1. B. E. Bayer, "Color imaging array," U.S. Patent 3971065, 1976.
2. B. Leung, G. Jeon, and E. Dubois, "Least-squares luma–chroma de- multiplexing algorithm for bayer demosaicking," IEEE Trans. Image Processing, vol. 20, no. 7, pp. 1885–1894, 2011.
3. B. Park and J. Jeong, "Color filter array demosaicking using densely connected residual network," IEEE Access, vol. 7, pp. 128076–128085, 2019.
4. H. J. Trussell and R. E. Hartwig, "Mathematics for demosaicking," IEEE Trans. Image Processing, vol. 11, no. 4, pp. 485–492, 2002.
5. H. S. Malvar, L.-w. He, and R. Cutler, "High-quality linear interpolation for demosaicing of bayer-patterned color images," in Proc. IEEE Int. Conf. Acoustics, Speech and Signal Processing, vol. 3, pp. 485–488, IEEE, 2004.
6. K.-H. Chung and Y.-H. Chan, "Color demosaicing using variance of color differences," IEEE Trans. Image Processing, vol. 15, no. 10, pp. 2944–2955, 2006.
7. L. Zhang, X. Wu, A. Buades, and X. Li, "Color demosaicking by local directional interpolation and nonlocal adaptive thresholding," J. Electron. Imag., vol. 20, no. 2, p. 023016, 2011.
8. N.-X. Lian, L. Chang, Y.-P. Tan, and V. Zagorodnov, "Adaptive filtering for color filter array demosaicking," IEEE Trans. Image Processing, vol. 16, no. 10, pp. 2515–2525, 2007.
9. W. Lu and Y.-P. Tan, "Color filter array demosaicking: new method and performance measures," IEEE Trans. Image Processing, vol. 12, no. 10, pp. 1194–1210, 2003.
10. X. Chen, G. Jeon, and J. Jeong, "A gradient inverse weighted filtering approach for video deinterlacing," IEICE Trans. Commun., vol. 95, no. 12, pp. 3933–3936, 2012.
11. X. Chen, L. He, G. Jeon, and J. Jeong, "Multidirectional weighted interpolation and refinement method for bayer pattern CFA demosaicking," IEEE Trans. Circuits and Systems for Video Technology, vol. 25, no. 8, pp. 1271–1282, 2014.
12. X. Luo, H. Sun, Q. Chen, J. Chen, and Y. Wang, "Real-time demosaicking of bayer pattern images," Chinese J. Optics Appl. Optics., vol. 3, no. 2, pp. 182–187, 2010.
13. Y. Wang, S. Yin, S. Zhu, Z. Ma, R. Xiong, and B. Zeng, "Ntsdcn: New three-stage deep convolutional image demosaicking network," IEEE Trans. Circuits and Systems for Video Technology, vol. 31, no. 9, pp. 3725–3729, 2020.